

Optical alignment and confinement of an ellipsoidal nanorod in optical tweezers: a theoretical study

Jan Trojek, Lukáš Chvátal, and Pavel Zemánek*

*Institute of Scientific Instruments of the ASCR, v.v.i., Academy of Sciences of the Czech Republic,
Královopolská 147, 612 64 Brno, Czech Republic*

*Corresponding author: zemanek@isibrno.cz

Received December 6, 2011; revised February 19, 2012; accepted March 9, 2012;
posted March 9, 2012 (Doc. ID 159516); published June 6, 2012

Within the Rayleigh approximation, we investigate the behavior of an individual ellipsoidal metal nanorod that is optically confined in three dimensions using a single focused laser beam. We focus on the description of the optical torque and optical force acting upon the nanorod placed into a linearly polarized Gaussian beam (scalar description of the electric field) or a strongly focused beam (vector field description). The study comprises the influence of the trapping laser wavelength, the angular aperture of focusing optics, the orientation of the ellipsoidal nanorod, and the aspect ratio of its principal axes. The results reveal a significantly different behavior of the nanorod if the trapping wavelength is longer or shorter than the wavelength corresponding to the longitudinal plasmon resonance mode. Published experimental observations are compared with our theoretical predictions with satisfactory results. © 2012 Optical Society of America

OCIS codes: 140.7010, 350.4855.

1. INTRODUCTION

Optical trapping of micrometer- and nanometer-scale particles by lasers has found many useful applications over the past two decades [1–3]. While optical trapping of microparticles is nowadays a very common tool in physical, biological, and chemical sciences, experimental extension to nanoparticles is not straightforward: the gradient force responsible for the trapping falls down with the particle volume and is easily overcome by thermal forces arising from molecular fluctuations of the surrounding medium.

Metallic nanoparticles can resolve the difficulties with the stability of optical trapping due to their larger refractive index relative to the surrounding medium, which leads to stronger optical trapping compared to dielectric nanoparticles at wavelengths longer than the localized surface plasmon resonance wavelength [4]. At the plasmon resonance wavelength, collective oscillations of conduction electrons lead to enhanced light absorption and scattering, and the optical trapping force changes significantly near this wavelength. Spherical metallic nanoparticles are localized at the beam axis for trapping wavelengths longer than the plasmon resonance wavelength but repelled from the axis for shorter trapping wavelengths [5,6]. The plasmon resonant wavelength can be tuned over a wide spectral range by varying the size and shape of the metallic particles [7]. Elongated nanoparticles tend to orient with respect to the polarization or propagation axis of the incident trapping beam [8–10]. By monitoring the polarized light emission from an individual gold nanorod (NR), it is possible to determine its orientation as a function of time [11]. The large signal-to-noise ratio, photochemical stability, nonblinking and nonbleaching, fast time response, and small size of these NRs make them ideal probes for orientation sensing in material science and molecular biology [12–14]. Gold NRs are easily taken up by mammalian cells and are frequently used in biological experiments [15].

Inorganic nanotubes have been successfully employed for sensing of single DNA molecule translocation in nanofluidic devices [16].

Optical control of the orientation and position of NRs enhances the possibilities of their applications. Holographic optical tweezers have been employed for trapping, deposition, and photochemical transformation of single wall carbon nanotubes [17]. NRs have been also utilized as light driven nanorotors [9,18]. Rotation of the beam polarization induced controlled NR rotation. Such a principle can be applied to control and manipulate important elements in nanoelectronics, such as nanotubes and nanowires, measure the local viscoelastic properties of biological and rheological systems, or perform torsional analysis experiments with biomolecules such as DNA [19]. Tiny volumes of NRs compared to conventional dielectric particles pave the way to study the mechanical heterogeneity of liquid environments on a nanoscale level. The rotational and translational motions of NRs can be detected using holographic video microscopy that also provides real time feedback for their three-dimensional (3D) micromanipulation [20]. The first quantitative measurements of the optical torque exerted on a single gold NR in a polarized 3D optical trap were presented by Ruijgrok *et al.* [21]. They determined the torque both by observing the time-averaged orientation distribution and by measuring the dynamics of the rotational Brownian fluctuations. Stable optical trapping of a single gold NR immersed in water was demonstrated for an objective lens with high NA and trapping wavelengths longer than the longitudinal plasmon resonances of the NRs [22,23]. The stiffness of a 3D optical trap was measured in the case of a single optically trapped gold NR [23]. It was shown in [23] that the optical forces correlate with NR polarizability, which depends on both the particle volume and its aspect ratio.

In this paper we present an in-depth theoretical study of NR behavior in a single focused Gaussian beam in both scalar and

vector descriptions. We focus on the orientation and lateral and longitudinal confinement of a single gold, silver, and silica NR, and we show that the usually used scalar field description (paraxial Gaussian beam) cannot explain optical trapping observed in the experiments mentioned above. However, more exact vector field description provides an optical potential well deep enough for stable confinement of NRs.

The paper is organized into logical steps leading to the determination of the stable orientations and positions of an ellipsoidal NR trapped by optical tweezers. Section 2 introduces three different descriptions of the incident focused laser beam and compares their spatial intensity distributions. Section 3 presents theoretical descriptions of optical force and torque acting upon the NR if the Rayleigh approximation and scalar or vector descriptions of the incident beam are applied. Section 4 analyzes step by step the NR behavior if the NR is illuminated by a linearly polarized focused beam. Again both the scalar and vector descriptions of the incident fields are compared. In Subsection 4.A the torques acting upon the NR are analyzed and the stable NR alignment is determined. In Subsection 4.B we assume the NR is localized on the optical axis and we look for its longitudinal stable position. Consequently, knowing the stable NR orientation and longitudinal position, in Subsection 4.C we analyze the stability of the lateral trapping if the NR is placed on the optical axis. Since, in contrast to spherical objects, the stability of the NR confinement is influenced by the NR orientation, we analyze in Subsection 4.D the stability of the NR optical trapping depending on the NR orientation. Since we consider metal NRs that absorb energy from the trapping beam and thus heat up, Section 5 analyzes the effects of temperature increase of the NR trapped by the laser beam. Section 6 compares presented theoretical results with experimental data published by other research groups.

2. DESCRIPTION OF THE INCIDENT LASER BEAM

Correct description of the laser beam focused by a high numerical aperture (NA) objective is a challenging topic [24–27], especially if optical aberrations are taken into account [28]. In this study we neglect the optical aberrations and focus on the two most frequently used descriptions: *scalar Gaussian beam* description (SD) [29] and *vector* description (VD) based on the Debye approximation of the plane wave diffraction on a circular aperture [25,26].

A. Scalar Beam Description

Let us consider a laser beam propagating in the medium of refractive index n_m along z -axis and polarized along x -axis. The beam is focused by a lens with an NA and an angular aperture Θ related as

$$\text{NA} = n_m \sin \Theta. \quad (1)$$

The electric field of a moderately focused beam can be described in the paraxial approximation as the scalar Gaussian beam [27,29]:

$$E_x(x, y, z) = E_0 \frac{w_0}{w(z)} \exp\left(\frac{-(x^2 + y^2)}{w^2(z)}\right) \times \exp\left(ikz + ik\frac{x^2 + y^2}{2R(z)} - i\zeta(z)\right), \quad (2)$$

$$E_y(x, y, z) = 0, \quad E_z(x, y, z) = 0, \quad (3)$$

where E_0 is the electric field intensity at the beam focus $x = y = z = 0$, $k = 2\pi/\lambda$ is the wavenumber, and λ is the beam wavelength in the surrounding medium of refractive index n_m . The following quantities denote the well-known parameters of the Gaussian beam: the beam width $w(z) = w_0 \sqrt{1 + (z/z_R)^2}$, the wave front radius $R(z) = z[1 + (z_R/z)^2]$, the Guoy phase $\zeta(z) = \arctan(z/z_R)$, the Rayleigh range $z_R = kw_0^2/2$, and the beam waist radius w_0 . Let us recall the beam waist is equal to the radial distance from the optical axis at the focal plane where the electric field intensity fulfills

$$|E_x(w_0, 0, 0)| = |E_x(0, w_0, 0)| = |E_x(0, 0, 0)|/e. \quad (4)$$

This paraxial scalar (zeroth-order) Gaussian beam approximation can be enhanced to higher orders by taking more terms in the Taylor expansion of the vector potential A when the Helmholtz equation for A is solved [27]. Such field description is generally vectorial. The fifth-order Gaussian beam approximation (G5) [27] is among the most frequently used descriptions related to the theoretical studies of optical forces acting upon particles [30]. Therefore we mention it here to link it to other descriptions used in this paper. The G5 approximation gives the same field distribution on the optical axis as SD; it has only a transversal electric field component in yz plane and an extra longitudinal field component in xz plane:

$$E(0, y, z) = [E_x^{G5}(0, y, z), 0, 0], \quad (5)$$

$$E(x, 0, z) = [E_x^{G5}(x, 0, z), 0, E_z^{G5}(x, 0, z)]. \quad (6)$$

B. Vector Beam Description

The following Debye approximation of the diffraction of a convergent spherical wave on a circular aperture [25,26] is considered as highly appropriate for the description of a strongly focused beam without aberrations:

$$E_x(x, y, z) = -\frac{i}{2}k \left(I_0 + I_2 \frac{x^2 - y^2}{x^2 + y^2} \right), \quad (7)$$

$$E_y(x, y, z) = -ikI_2 \frac{xy}{x^2 + y^2}, \quad (8)$$

$$E_z(x, y, z) = -kI_1 \frac{x}{\sqrt{x^2 + y^2}}, \quad (9)$$

where

$$I_0(r, z, \Theta) = \int_0^\Theta A(\alpha) \sin \alpha (1 + \cos \alpha) J_0(kr \sin \alpha) \exp(ikz \cos \alpha) d\alpha, \quad (10)$$

$$I_1(r, z, \Theta) = \int_0^\Theta A(\alpha) \sin^2 \alpha J_1(kr \sin \alpha) \exp(ikz \cos \alpha) d\alpha, \quad (11)$$

$$I_2(r, z, \Theta) = \int_0^\Theta A(\alpha) \sin \alpha (1 - \cos \alpha) J_2(kr \sin \alpha) \exp(ikz \cos \alpha) d\alpha, \quad (12)$$

where $r = \sqrt{x^2 + y^2}$ denotes the radial distance from the optical axis z , J_n denotes the Bessel function of the first kind and n th order, and the angular amplitude distribution in the aplanatic projection follows [26]

$$A(\alpha) = A_0 \sqrt{\cos \alpha}. \quad (13)$$

The amplitude A_0 can be related to the electric field intensity at the beam focus $E_x(0, 0, 0)$ using Eqs. (7)–(10):

$$E_x(0, 0, 0) = \frac{k}{15} A_0 (8 - 3 \cos^{5/2} \Theta - 5 \cos^{3/2} \Theta). \quad (14)$$

Equation (14) thus enables a direct comparison of the vector and the scalar beam descriptions if we set the electric field intensity at the beam focus identical in both cases, i.e., $E_0 = E_x(0, 0, 0)$. Furthermore, one can immediately conclude that the vector beam has only E_x -component in yz plane. This property enables a direct comparison of lateral profiles of both fields assuming that the effective Gaussian beam waist w_0 for the SD model corresponds to the radial position where the vector beam satisfies $|E_x(0, w_0, 0)| = |E_x(0, 0, 0)|/e$. Figure 1 compares the beam intensity profiles in all considered approximations SD, G5, and VD for different angular apertures Θ . The top left plot of $|E(x, 0, 0)|$ reveals noticeable differences between all models along the direction of the beam polarization. The bottom left plot demonstrates negligible differences in the higher values of the electric field intensity profiles $|E(0, y, 0)|$ between all three compared models along y -axis. The plots of the longitudinal field intensity profiles $|E(0, 0, z)|$ in the right column prove stronger longitudinal field gradients (D_z) obtained from VD.

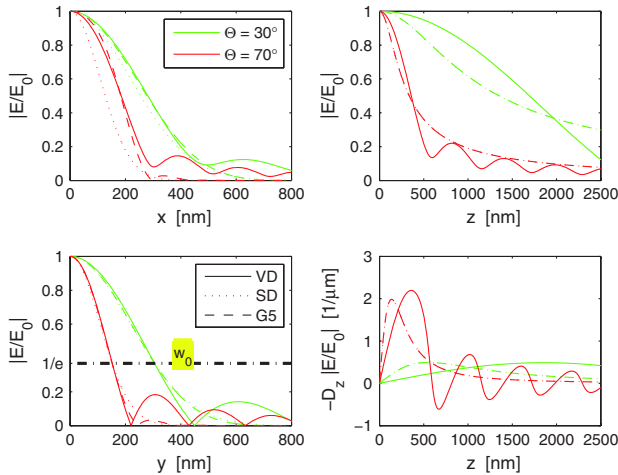


Fig. 1. (Color online) Comparison of three different descriptions of the incident laser beam. Normalized profiles of the absolute values of the electric field intensity in the incident beam along x (top left), y (bottom left), and z (top right) axis are shown for the vector description [VD—solid, Eqs. (7)–(9)], the scalar description [SD—dot, Eq. (2)], and the fifth-order description [G5—dash, Eq. (27)]. Beam waist w_0 (corresponding to the radial distance along y -axis where $|E| = |E_0|/e$, which is denoted by the dash-dotted line) is identical for all considered approximations, and two different angular apertures of the VD beam, $\Theta = 30^\circ$ (green) and $\Theta = 70^\circ$ (red), are studied. The electric field is normalized to its absolute value at the beam focus $|E_0|$. The negative gradient ($-D_z$) of the longitudinal field is plotted along the optical axis z (bottom right). The following quantities and values are used in the calculations: vacuum laser wavelength $\lambda_0 = 500$ nm, $n_m = 1.33$.

3. OPTICAL FORCES AND TORQUES

In this study, we focus on finding the general rules for the behavior of NR in a focused laser beam and therefore we look for an analytical description of the force interaction between the NR and the laser beam. We adopt the simple Rayleigh approximation, which is only valid for an NR much smaller compared to the trapping wavelength, so that the electromagnetic field inside the NR can be considered constant. In the case of larger NRs, mainly numerical methods based on the transition matrix (T-matrix) approach [31–34] are used to investigate optical trapping in the focal region of a high NA optical system. Radiation torque and trapping force on highly elongated linear chains formed from nanospheres were also studied by the means of the T-matrix approach [35]. It was found that the shortest chains were stably oriented transversely to the optical axis, whereas the longest ones aligned themselves along the optical axis. Very good agreement between the T-matrix and the finite difference time domain (FDTD) methods has been reported by Simpson *et al.* [34] for different symmetry groups of nanoparticles. Also the coupled dipole method (CDM) was used to compute optical torque acting upon a micropropeller illuminated by a circularly polarized plane wave [36]. In contrast to the above numerical models, the rigorous diffraction theory can be used only in some special cases of particle geometry, e.g., for elliptically shaped dielectric nanocylinders [37,38].

A. Rayleigh Approximation

Assuming an NR is much smaller compared to the wavelength (NR length $l \ll \lambda$), the components of the optical force F_ξ (with $\xi = x, y, z$) and the optical torque M_ξ acting on such an NR are given by the following formulas [10,34,39,40]:

$$F_\xi = \frac{1}{2} \Re \{ \mathbf{p}^* \cdot \partial_\xi \mathbf{E} \}, \quad (15)$$

$$M_\xi = \frac{1}{2} \Re \{ \mathbf{p}^* \times \mathbf{E} \}_\xi, \quad (16)$$

where $\mathbf{p} = \hat{\alpha} \mathbf{E}$ is the dipole moment of the NR induced by the beam and $\hat{\alpha}$ denotes the polarizability tensor.

B. Polarizability Tensor of an Ellipsoidal Nanorod

Let us consider an ellipsoidal NR with semiaxes a, b, c and volume $V = 4\pi abc/3$. The polarizability α_j along the j -axis of the ellipsoid is given by [41,42]

$$\alpha_j = \frac{\alpha_j^0}{1 - \frac{\alpha_j^0}{6\pi\epsilon}}, \quad \alpha_j^0 = \frac{\epsilon_0 n_m^2 V}{L_j + \frac{1}{m^2 - 1}}, \quad m = \frac{n_p}{n_m}, \quad (17)$$

$$L_1 = \int_0^\infty \frac{abcds}{2(s+a^2)^{3/2}(s+b^2)^{1/2}(s+c^2)^{1/2}}, \quad (18)$$

where n_p is the refractive index of the NR, n_m is the refractive index of the surrounding medium, and the same formula [Eq. (18)] is valid for L_2 and L_3 with cyclical exchanges of index and axis.

In the case of an ellipsoidal NR with one long axis l_L and two identical short axes l_S , the polarizability tensor has the following form in its principal axes coordinate system:

$$\hat{\alpha} = \begin{vmatrix} \alpha'_L + i\alpha''_L & 0 & 0 \\ 0 & \alpha'_S + i\alpha''_S & 0 \\ 0 & 0 & \alpha'_S + i\alpha''_S \end{vmatrix}, \quad (19)$$

with real components α'_L , α''_L , α'_S , α''_S calculated from Eqs. (17) and (18).

We assume the NR is initially oriented with its long axis L parallel to the polarization of the beam, i.e., along the x -axis. The general orientation of the NR in the coordinate system x, y, z connected to the incident beam is described using the azimuthal angle ψ and the polar angle θ (see Fig. 2). The principal axes of the NR correspond to the axes of the rotated system of coordinates $x''y''z''$, where the NR long axis is oriented along the x'' -axis. Consequently, the transformation matrix between the coordinate systems $xyz \rightarrow x''y''z''$ has the following form:

$$\hat{R} = \begin{vmatrix} \cos \theta & 0 & -\sin \theta \\ 0 & 1 & 0 \\ \sin \theta & 0 & \cos \theta \end{vmatrix} \begin{vmatrix} \cos \psi & \sin \psi & 0 \\ -\sin \psi & \cos \psi & 0 \\ 0 & 0 & 1 \end{vmatrix}, \quad (20)$$

where both angles increase in accordance with the right hand rule.

The polarizability tensor of the rotated NR in the system of coordinates xyz is then done by the matrix product

$$\hat{A} = \hat{R}^{-1} \hat{\alpha} \hat{R}, \quad (21)$$

and the NR dipole moment \mathbf{p} excited by the total electric field \mathbf{E} at the NR position $\mathbf{r} = [x, y, z]$ is

$$\mathbf{p} = \hat{A}(\psi, \theta) \mathbf{E}(x, y, z). \quad (22)$$

C. Optical Force and Torque in a Paraxial Gaussian Beam

In order to obtain the simplest analytical expressions for the optical force and the optical torque acting upon an ellipsoidal NR, we first consider an incident Gaussian beam given by the scalar description in Eq. (2) and use it in Eqs. (15) and (16):

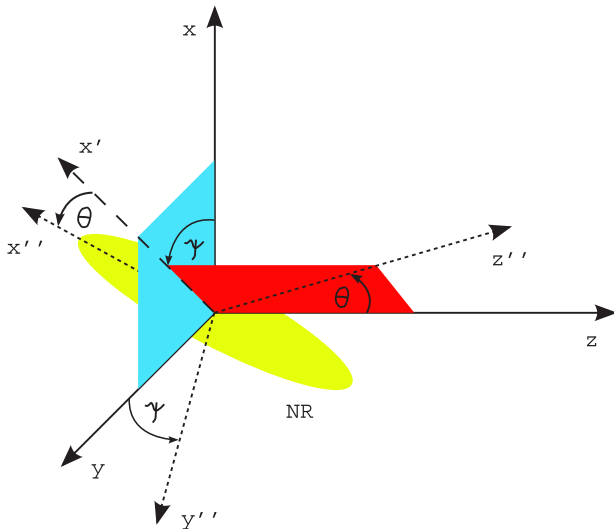


Fig. 2. (Color online) Orientation of the nanorod (NR) in the initial coordinate system xyz and the rotated coordinate system $x''y''z''$. The NR long axis is parallel to x'' -axis. The axis x' denotes the projection of the axis x'' to the plane xy .

$$F_x(x, y, z, \psi, \theta) = -E_0^2 \frac{z_R^2 k x}{2(z_R^2 + z^2)^2} \exp \left[-\frac{k z_R (x^2 + y^2)}{z_R^2 + z^2} \right] [a'(\psi, \theta) z_R - a''(\psi, \theta) z], \quad (23)$$

$$F_y(x, y, z, \psi, \theta) = -E_0^2 \frac{z_R^2 k y}{2(z_R^2 + z^2)^2} \exp \left[-\frac{k z_R (x^2 + y^2)}{z_R^2 + z^2} \right] [a'(\psi, \theta) z_R - a''(\psi, \theta) z], \quad (24)$$

$$F_z(x, y, z, \psi, \theta) = -E_0^2 \frac{z_R^2}{4(z_R^2 + z^2)^3} \exp \left[-\frac{k z_R (x^2 + y^2)}{z_R^2 + z^2} \right] \times \{ -2k a''(\psi, \theta) z^4 + 2a'(\psi, \theta) z^3 + (k x^2 + k y^2 - 4k z_R^2 + 2z_R) a''(\psi, \theta) z^2 - [2k z_R (x^2 + y^2) - 2z_R^2] a'(\psi, \theta) z - [k z_R^2 (x^2 + y^2) + 2k z_R^4 - 2z_R^3] a''(\psi, \theta) \}; \quad (25)$$

$$M_x(x, y, z, \psi, \theta) = 0, \quad (26)$$

$$M_y(x, y, z, \psi, \theta) = -E_0^2 \frac{z_R^2}{4(z_R^2 + z^2)} \exp \left[-\frac{k z_R (x^2 + y^2)}{z_R^2 + z^2} \right] \times (\alpha'_L - \alpha'_S) \sin 2\theta \cos \psi, \quad (27)$$

$$M_z(x, y, z, \psi, \theta) = -E_0^2 \frac{z_R^2}{4(z_R^2 + z^2)} \exp \left[-\frac{k z_R (x^2 + y^2)}{z_R^2 + z^2} \right] \times (\alpha'_L - \alpha'_S) \sin 2\psi \cos^2 \theta, \quad (28)$$

where

$$a'(\psi, \theta) = \alpha'_S + (\alpha'_L - \alpha'_S) \cos^2 \theta \cos^2 \psi, \quad (29)$$

$$a''(\psi, \theta) = \alpha''_S + (\alpha''_L - \alpha''_S) \cos^2 \theta \cos^2 \psi. \quad (30)$$

The torque expression (28) for $x = y = z = 0$ and $\theta = 0$ exactly agrees with the analogical one from the appendix in [10], where the authors considered an incident plane wave and only a two-dimensional rotation of the NR. More general 3D rotation of a spheroid placed at the focus of a Gaussian beam was published in [43]. Although they chose another way to describe the NR spatial orientation, their torque vector also matches with Eq. (28) for $x = y = z = 0$.

Since in the text below we consider the particles are optically trapped on the optical axis, let us simplify the expressions accordingly:

$$\begin{aligned} F_x(0, 0, z, \psi, \theta) &= 0, \\ F_y(0, 0, z, \psi, \theta) &= 0, \\ M_x(0, 0, z, \psi, \theta) &= 0, \end{aligned} \quad (31)$$

$$F_z(0, 0, z, \psi, \theta) = E_0^2 \frac{z_R^2}{2(z_R^2 + z^2)^2} [a''(\psi, \theta) k (z_R^2 + z^2) - a'(\psi, \theta) z - a''(\psi, \theta) z_R]; \quad (32)$$

$$M_y(0, 0, z, \psi, \theta) = -E_0^2 \frac{z_R^2}{4(z_R^2 + z^2)} (\alpha'_L - \alpha'_S) \sin 2\theta \cos \psi, \quad (33)$$

$$M_z(0, 0, z, \psi, \theta) = -E_0^2 \frac{z_R^2}{4(z_R^2 + z^2)} (\alpha'_L - \alpha'_S) \sin 2\psi \cos^2 \theta. \quad (34)$$

Physical consequences coming from these equations are discussed in Section 4.

D. Optical Force and Torque in a Tightly Focused Beam

We use the vector description of the beam presented in Subsection 2.B and insert it into Eqs. (15) and (16). If we again assume the NR is placed on the optical axis, only the x -component of the electric field E is nonzero, and we obtain for the components of the force and torque

$$\begin{aligned} F_x(0, 0, z, \psi, \theta) &= 0, \\ F_y(0, 0, z, \psi, \theta) &= 0, \\ M_x(0, 0, z, \psi, \theta) &= 0, \end{aligned} \quad (35)$$

$$F_z(0, 0, z, \psi, \theta) = \frac{1}{2} \Re \{ [a'(\psi, \theta) + ia''(\psi, \theta)]^* \times E_x(0, 0, z)^* \partial_z E_x(0, 0, z) \}; \quad (36)$$

$$M_y(0, 0, z, \psi, \theta) = -\frac{1}{4} |E_x(0, 0, z)|^2 (\alpha'_L - \alpha'_S) \sin 2\theta \cos \psi, \quad (37)$$

$$M_z(0, 0, z, \psi, \theta) = -\frac{1}{4} |E_x(0, 0, z)|^2 (\alpha'_L - \alpha'_S) \sin 2\psi \cos^2 \theta. \quad (38)$$

4. NANOROD OPTICAL ALIGNMENT AND CONFINEMENT

A. Stable Alignment of the Nanorod

If we compare Eqs. (33) and (34) with Eqs. (37) and (38), one immediately sees that the torque components have the same dependence on the NR orientation (angles θ and ψ) and shape ($\alpha'_L - \alpha'_S$). Therefore, there would be no difference between the NR rotation if the NR were placed on the optical axis and the scalar Gaussian beam or the focused vector beam description were used. Stable alignment of the NR in the beam is done by the torque equal to zero and the negative derivative of the torque components with respect to the related angles. As we can see, such stable orientations do not depend on the NR position along z -axis and, therefore, they can be investigated independently of the stable longitudinal position of the trapped NR. A careful inspection of the torque equations reveals two stable orientations of the NR with respect to the direction of the incident electric field (light polarization); these orientations depend on the sign of the polarizability difference ($\alpha'_L - \alpha'_S$). Table 1 summarizes the results, and it also

expresses the forms of parameters a' , a'' from Eqs. (29) and (30) for the two cases of the stable NP orientation. The specific form of a' , a'' then significantly influences the optical forces acting upon the NR.

The sign of the polarizability difference ($\alpha'_L - \alpha'_S$) depends on the wavelength used for the NR illumination. As Fig. 3 demonstrates for NRs made of three materials, there exist spectral regions of different stable NR orientations with respect to the polarization of the incident beam. In the long wavelength region $\alpha'_L > \alpha'_S$, the NR is aligned parallel to the electric field E of the incident beam. Conversely, in the short wavelength region $\alpha'_S > \alpha'_L$, the NR aligns perpendicular to the electric field E of the incident beam. Surprisingly, the dielectric silica NR can also switch from the parallel to the perpendicular orientation although there is no plasmon resonance in this material. In the investigated range of wavelengths, gold and silica enable one NR reorientation; however, silver reveals a more complex NR behavior with three NR reorientations.

The NR reorients at the wavelength λ'_0 that satisfies $\alpha'_L(\lambda'_0) = \alpha'_S(\lambda'_0)$. However, this wavelength depends on the ratio of short l_S and long l_L -axis of the ellipsoidal NR. Figure 4 reveals that in the case of metallic NRs, there can be more than one λ'_0 for certain ratios l_S/l_L . In the case of Au NR, λ'_0 overlaps with the wavelength of the plasmon resonance along the long NR axis. For Ag NR, λ'_0 coincides with the plasmon resonances along long and short NR axes. Although there is no plasmon resonance in the case of dielectric silica NRs, the wavelength λ'_0 coincides well with the maximum of imaginary part of the NR polarizability, too. Figure 4 then plainly reveals that the long-axis plasmon resonance in metal NR determines the longest wavelength where the NR reorients.



B. Longitudinal Trapping

We have concluded in the previous part that the NR orientation does not depend on the longitudinal position of the NR. In this subsection, we investigate conditions for stable longitudinal confinement of an NR placed on the optical axis. Using Eq. (32), which describes the longitudinal optical force in the scalar Gaussian beam approximation, one can find one stable z_0 and one unstable z'_0 equilibrium positions of the NR, independent on the trapping field intensity:

$$\begin{aligned} z_0 &= \frac{a' - \sqrt{D}}{2ka''}, & z'_0 &= \frac{a' + \sqrt{D}}{2ka''}, \\ D &= (a')^2 + 4(a'')^2 k z_R (1 - k z_R). \end{aligned} \quad (39)$$

However, they exist only if the discriminant D is positive, $D > 0$, i.e., in a tightly focused beam. If the optical confinement is to be stable against thermal fluctuations of the surrounding medium, the work needed to get the NR from z_0 to $z'_0 > z_0$ must be higher than the energy of the thermal motion $k_B T$, where k_B is the Boltzmann constant and T is the absolute temperature:

Table 1. Physical Conditions for the Stable Alignment of the Nanorod Corresponding to its Parallel \parallel and Perpendicular \perp Orientation with Respect to the Electric Field E of the Incident Beam

E direction	NR orientation	symbol	α	ψ	θ	a'	a''
\uparrow		\parallel	$\alpha'_L > \alpha'_S$	0	0	α'_L	α'_L
\uparrow		\perp	$\alpha'_L < \alpha'_S$	0	$\frac{\pi}{2}$	α'_S	α'_S

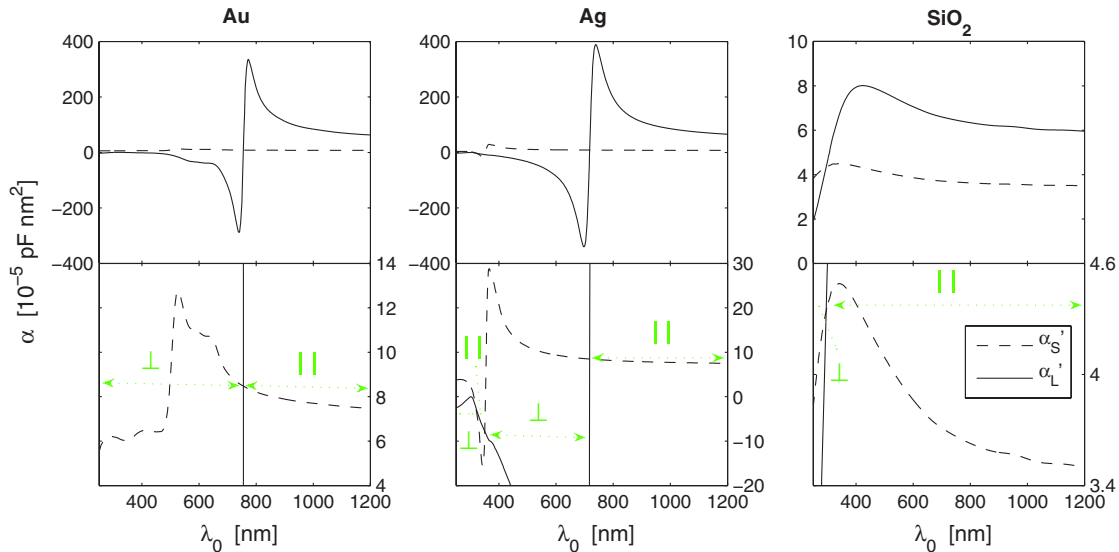


Fig. 3. (Color online) Spectral dependence of the polarizabilities α'_L and α'_S described by Eq. (17). The bottom row presents the same data as the top row with a different scaling of the vertical axis. Spectral regions where $(\alpha'_L - \alpha'_S)$ does not change its sign are denoted by the horizontal green arrows. In these regions, the NR is aligned parallel to the beam polarization by its long axis (marked as \parallel) or short axis (marked as \perp). We consider ellipsoidal Au, Ag, and SiO_2 NRs with long axis $l_L = 40$ nm and short axes $l_S = 10$ nm immersed in water. The values of the refractive indices are taken from [44].

$$U_z = - \int_{z_0}^{z'_0} F_z(0, 0, z) dz > k_B T. \quad (40)$$

Within the considered scalar description, the work U_z can be found in the analytical form

$$U_z = \frac{1}{4} E_0^2 \left[\sqrt{D} - a''(2kz_R - 1) \arctan \frac{\sqrt{D}}{a''(2kz_R - 1)} \right]. \quad (41)$$

Because of the stochastic nature of the NR motion, the higher the ratio $U_z/(k_B T)$, the longer the so-called first mean passage time [45] (under certain conditions also called Kramers time [46]) corresponding to the mean time needed by the particle to escape across z'_0 .

Considering the vector description of the Gaussian beam, the analyses must be done numerically. Figure 5 compares the longitudinal position of the optical trap obtained from Eq. (39) and from numerical analysis of Eq. (36) for gold NR. The illumination wavelength and the angular aperture are

chosen as the free parameters; however, the wavelength range is chosen such that the NR reaches stable alignment with respect to the beam polarization (see Table 1 and Fig. 3). The white regions denote a combination of parameters where no stable longitudinal equilibrium position (optical trap) exists. Comparing the results from the scalar and vector beam descriptions, one can immediately see that the vector description provides optical traps even for low angular apertures and wavelengths closer to the plasmon resonance. At the same time, the optical traps are longitudinally more displaced from the beam focus in the vector description. This corresponds to the different longitudinal profiles of the optical intensity of Gaussian beams described by SD and VD, as Fig. 1 demonstrated. However, both descriptions predict no longitudinal NR confinement for red detuned wavelengths in the vicinity of the plasmon resonance and for angular apertures Θ lower than about 20 deg. Since the optical forces and torques are directly proportional to the incident laser power, we choose for all the figures the same intensity of the electric

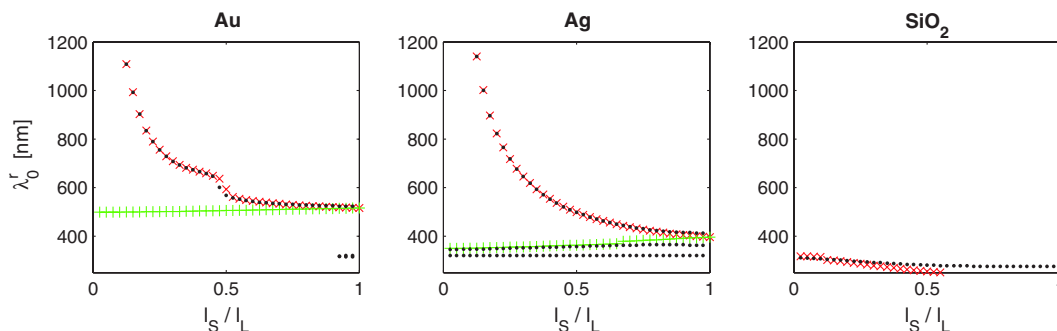


Fig. 4. (Color online) Critical parameters under which the NR reorients. The ratio of lengths of the short l_S and long l_L -axis of the ellipsoidal NR determines the wavelength λ_0^r at which $(\alpha'_L - \alpha'_S = 0)$ and the NR reorients (black dots). For comparison, the combinations of l_S/l_L and λ_0^r for which the imaginary part of the NR polarizability α'_L and α'_S reaches maximum are denoted by a red \times and a green $+$, respectively. In the case of metal NRs, they correspond to the plasmon resonances along the long or short NR axis, respectively. We again consider Au, Ag, and SiO_2 NRs immersed in water and having long axis lengths equal to $l_L = 40$ nm.

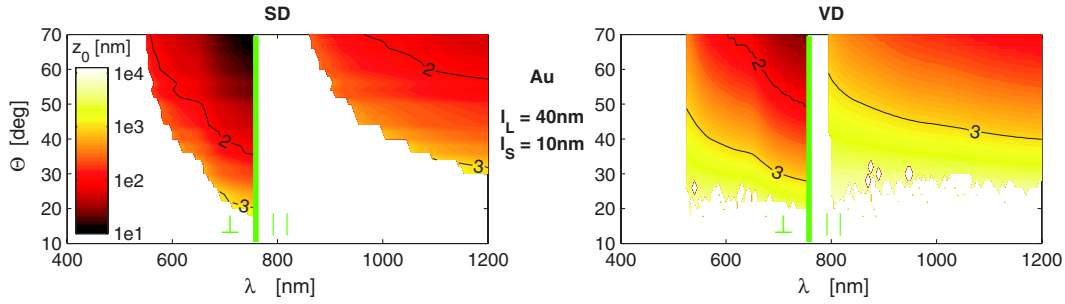


Fig. 5. (Color online) Longitudinal equilibrium positions z_0 of Au NR as a function of the vacuum trapping wavelength λ_0 and the angular aperture Θ . The scalar (SD, left) and vector (VD, right) descriptions of the incident Gaussian beam are compared; contours of identical z_0 are in logarithmic scale. The vertical green line divides the range of wavelengths into two regions where the NR is oriented by its long axis parallel (\parallel) or perpendicular (\perp) to the beam polarization (along x -axis). No equilibrium positions z_0 exist for parameters falling into the white regions. The intensity of the electric field at the beam focus E_0 was equal to $E_0 = 19$ MV/m; the Au NR of the dimensions $l_L = 40$ nm and $l_S = 10$ nm was immersed in water.

field at the beam focus $E_0 = 19$ MV/m. It corresponds to the optical intensity $I_0 = 637$ mW/ μm^2 , which is obtained if the laser power of 1 W is focused into the beam waist $w_0 = 1$ μm .

Figure 6 compares the work U_z needed to free the NR longitudinally for the scalar and vector descriptions of the incident Gaussian beams. One can find that the vector description provides slightly higher values of U_z and consequently more stable longitudinal NR confinement. One also immediately recognizes that the NR confinement is much weaker below the plasmon resonance (at shorter wavelengths), i.e., if the NR long axis is oriented perpendicularly to the beam polarization. This corresponds to our previous results in Eqs. (29) and (30) and Table 1 because for this NR orientation, much weaker polarizabilities α'_S and α'_L are responsible for the magnitude of the optical force.

C. Lateral Trapping

In the previous parts, we have assumed without a proof that the NR is placed on the optical axis. In this part, we focus on the lateral stability of the trapped NR. Let us assume first the scalar description of the incident Gaussian beam using Eqs. (23)–(25), and let us express the lateral work U_r needed to move the NR from the beam axis to infinity (so-called lateral depth of the optical trap):

$$U_r = - \int_0^\infty F_r(r, z) dr = E_0^2 \frac{z_R (a' z_R - a'' z)}{4(z_R^2 + z^2)} = K_r \frac{z_R^2 + z^2}{2kz_R}, \quad (42)$$

where F_r and K_r denote the lateral optical force and trap stiffness, respectively. Since the force F_r does not change its sign for all radial distances r at a fixed z , positive values of U_r

indicate the NR is confined at the optical axis. However, for certain wavelengths and longitudinal positions, the bracket ($a' z_R - a'' z$) can become negative and, subsequently, the NR will be repelled from the optical axis. This happens if $z > z_R a' / a''$, assuming positive a'' (note that a'' varies in the range between α'_S and α'_L depending on the NR orientation; therefore $a'' > 0$). A detailed analysis for the scalar Gaussian beam reveals that the longitudinal stable equilibrium position of the optical trap z_0 , done by Eq. (39), always satisfies $z_0 < z_R a' / a''$. If $a' \leq 0$, there is no stable longitudinal position z_0 , and the NR is repelled from the optical axis. Therefore, we can conclude that the NR is stably trapped laterally on the optical axis if the NR is stably aligned with respect to the beam polarization and stably trapped longitudinally.

Figure 7 compares the lateral works for the scalar and vector descriptions of the incident Gaussian beam. The comparison of the top left panel of Fig. 7 with the left panel of Fig. 6 calculated for the scalar beam description proves that once the NR is trapped longitudinally, it is also trapped laterally because the lateral work is always positive. However, the vector description diverts from this rule for lower angular apertures near the plasmon resonance, as illustrated by the comparison of the remaining three panels of Fig. 7 with the right panel of Fig. 6. In this region, the NR can be trapped longitudinally; however, it will be repelled from the optical axis. A similar effect was observed by Simpson and Hanna [47] in the case of a dielectric microrod optically trapped in a tightly focused Gaussian beam. They calculated the coupling between lateral translations and rotations of the rod, which rose from the asymmetry of the stiffness matrix, and they showed that the rod was laterally repelled from the optical axis for certain rod orientations.

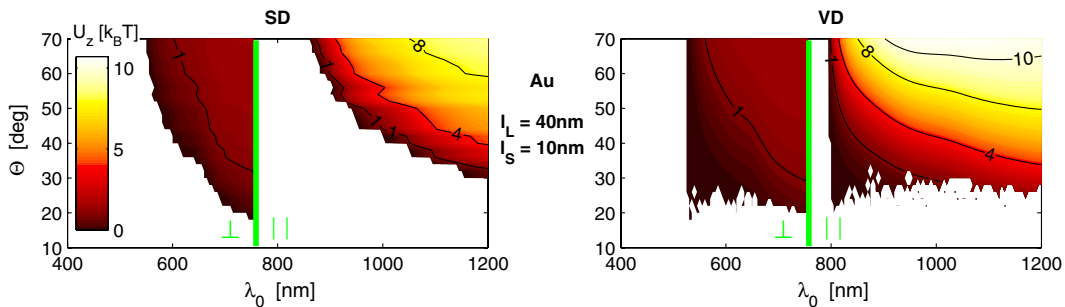


Fig. 6. (Color online) The work U_z needed to free the Au NR in longitudinal direction as a function of the vacuum trapping wavelength λ_0 and the angular aperture Θ . The same conditions and symbols are used as in Fig. 5.

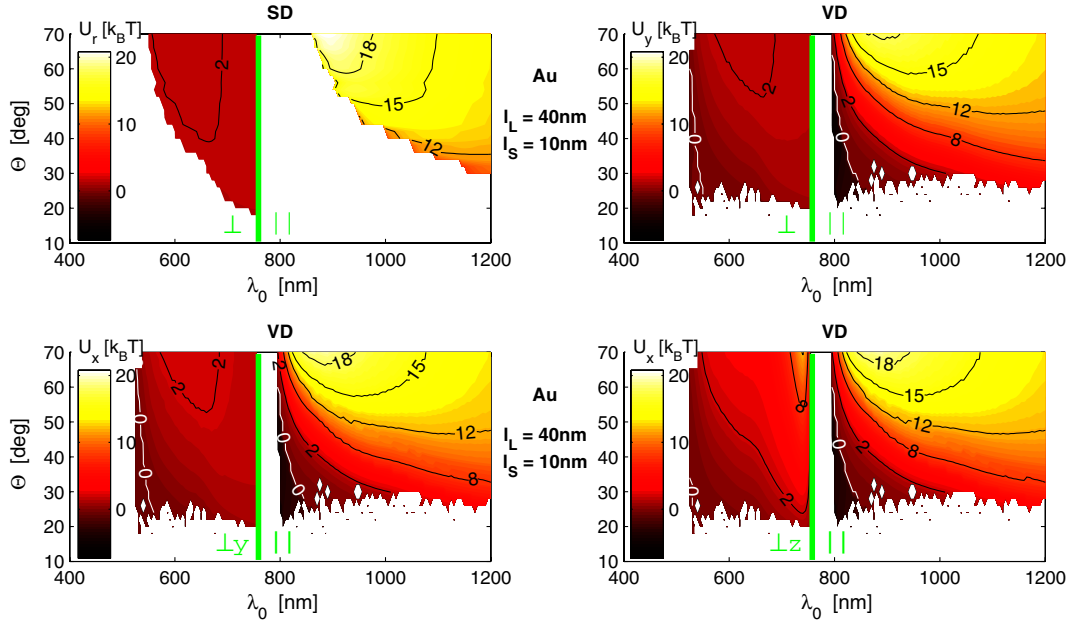


Fig. 7. (Color online) The work needed to transfer the NR from the optical axis to infinity in the lateral direction as a function of the vacuum trapping wavelength λ_0 and the angular aperture Θ . The optical trap is laterally symmetrical in the scalar description (SD) and, therefore, the work is denoted as U_r , and expressed by Eq. (42). However, in the vector description, the work generally differs for the NR transport along x and y -axis, denoted as U_x and U_y , respectively. In the case of U_x , two orientations of the NR must be considered, along y -axis (\perp_y) and z -axis (\perp_z). The same conditions and symbols are used as in Fig. 5.

D. Stability of the Nanorod Orientation

Up to now, we have mainly assumed that the NR is oriented parallel or perpendicularly to the beam polarization, but we have not addressed the stability of such NR orientation. Let us suppose the NR is trapped on the optical axis at the equilibrium position z_0 and that it is aligned parallel or perpendicularly to the beam polarization. The work needed to deflect the NR from its equilibrium alignment ψ_0, θ_0 (see Table 1) by an angle δ is expressed as

$$\begin{aligned} U_R^\psi &= - \int_{\psi_0}^{\psi_0+\delta} M_z(0, 0, z_0, \psi, 0) d\psi, \\ U_R^\theta &= - \int_{\theta_0}^{\theta_0+\delta} M_y(0, 0, z_0, 0, \theta) d\theta. \end{aligned} \quad (43)$$

It results in a general form

$$U_R = \frac{1}{4} |E_x(0, 0, z_0)|^2 |\alpha'_L - \alpha'_S| \sin^2 \delta. \quad (44)$$

Figure 8 compares this quantity calculated for $\delta = \pi/2$ and both descriptions of the incident Gaussian beams and for such combination of parameters that ensures the longitudinal NR confinement. Therefore, the white areas correspond again to such sets of parameters that do not provide longitudinal NR confinement. The numerical values reveal that the work U_R needed to reorient the NR by $\pi/2$ from its equilibrium orientation is typically equal to tens of $k_B T$. This value is high enough to keep the NR aligned stably against the thermal activation of the Brownian motion at room temperature T and considered incident field intensity E_0 .

However, the NR can still suffer from small deflections from its stable alignment due to the thermal activation. Since the polarizability a' from Eq. (29) depends on the NR orientation, the optical forces [expressed by Eqs. (23)–(25) and (36)] acting upon the NR depend on the NR orientation, too, and the analysis becomes practically intractable. Therefore, let us focus here only on the lateral and longitudinal trap stiffnesses at the equilibrium position $r_0 = [0, 0, z_0]$ and investigate how they are influenced by the NR alignment.

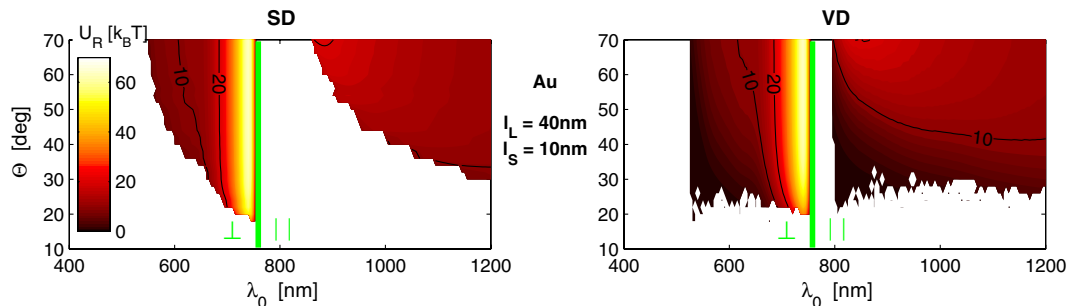


Fig. 8. (Color online) The work U_R needed to reorient the NR from the equilibrium position by $\pi/2$ as a function of the vacuum trapping wavelength λ_0 and the angular aperture Θ . The same conditions and symbols are used as in Fig. 5.

In the case of the scalar description, the lateral trap stiffnesses along x and y -axis are identical and can be expressed as

$$K_r = E_0^2 k z_R^2 \frac{a' z_R - a'' z}{2(z_R^2 + z^2)^2}. \quad (45)$$

In connection with Eq. (42), the NR behavior has been discussed for a stable alignment of the NR. However, the lateral stiffness K_r changes its sign for certain NR orientations and, consequently, the NR is repelled from the optical axis. Figure 9, top left, demonstrates such modification of the lateral stiffness K_r during deflection of the Au NR from its equilibrium alignment for both stable NR orientations (\parallel and \perp). In the parallel case (\parallel) the stiffness K_r decreases with increasing NR deflection but stays positive and, therefore, the NR stays confined on the optical axis. In the perpendicular case (\perp), the lateral stiffness changes its sign to negative even for small NR deflections (about 10 deg) and causes the NR repulsion from the optical axis.

A similar NR behavior is also observed in the vector description of the incident Gaussian beam, exploiting Eq. (47). The vector description of the incident beam also enables us to express the stiffnesses as a function of z -coordinate analytically:

$$K_x(z) = -\partial_x F_x(x, y, z)|_{y=0}^{x=0} = \frac{1}{32} k^4 \Re\{a_x H_1 H_3^* - 4a_z H_2 H_2^*\}, \quad (46)$$

$$K_y(z) = -\partial_y F_y(x, y, z)|_{y=0}^{x=0} = \frac{1}{32} k^4 \Re\{a_x H_1 H_4^*\}, \quad (47)$$

$$K_z(z) = -\partial_z F_z(x, y, z)|_{y=0}^{x=0} = \frac{1}{8} k^4 \Re\{a_x (H_1 H_6^* - H_5 H_5^*)\}, \quad (48)$$

where a_ξ denotes the polarizability of the NR along ξ -axis and the integrals H_n have the form

$$H_1(z) = \int_0^\Theta A(\alpha) \sin \alpha (1 + \cos \alpha) \exp(ikz \cos \alpha) d\alpha, \quad (49)$$

$$H_2(z) = \int_0^\Theta A(\alpha) \sin^3 \alpha \exp(ikz \cos \alpha) d\alpha, \quad (50)$$

$$H_3(z) = \int_0^\Theta A(\alpha) \sin^3 \alpha (1 + 3 \cos \alpha) \exp(ikz \cos \alpha) d\alpha, \quad (51)$$

$$H_4(z) = \int_0^\Theta A(\alpha) \sin^3 \alpha (3 + \cos \alpha) \exp(ikz \cos \alpha) d\alpha, \quad (52)$$

$$H_5(z) = \int_0^\Theta A(\alpha) \sin \alpha \cos \alpha (1 + \cos \alpha) \exp(ikz \cos \alpha) d\alpha, \quad (53)$$

$$H_6(z) = \int_0^\Theta A(\alpha) \sin \alpha \cos^2 \alpha (1 + \cos \alpha) \exp(ikz \cos \alpha) d\alpha. \quad (54)$$

No significant differences are observed between K_x and K_y values for the selected parameters, and therefore only K_y is plotted in Fig. 9, top right.

Figure 9, bottom row, also presents longitudinal trap stiffness K_z , which is obtained numerically at the NR equilibrium position $\mathbf{r}_0 = [0, 0, z_0]$. Noticeable differences between the scalar and vector descriptions are caused by different NR equilibrium positions z_0 (see Fig. 5). Similarly to the lateral

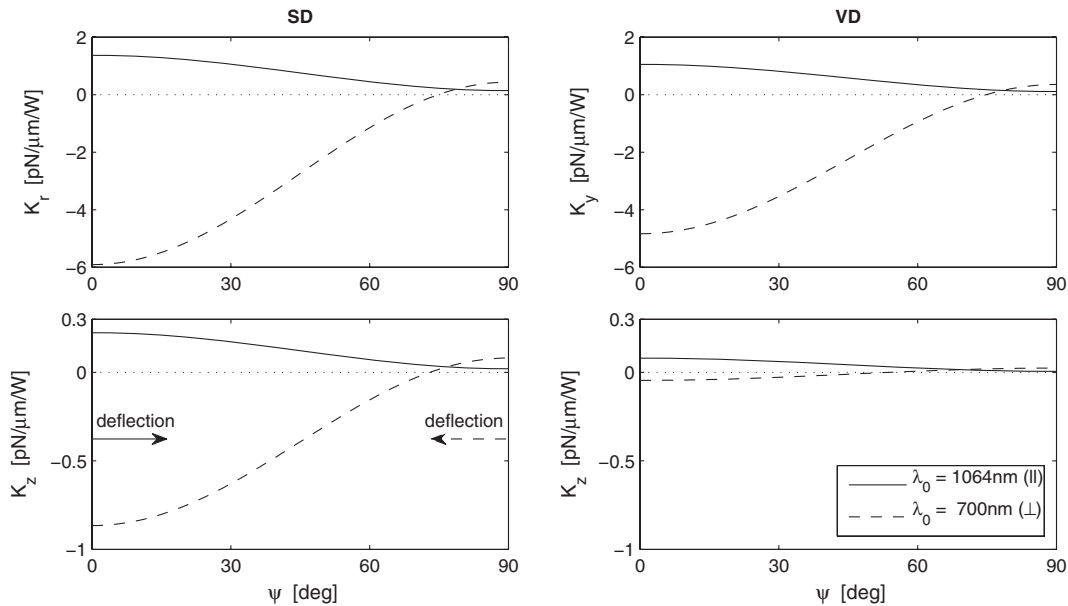


Fig. 9. Dependence of the lateral (K_r , K_y) and longitudinal (K_z) stiffnesses on the deflection ψ of the NR from its equilibrium alignment. The NR is deflected around the optical axis z by the azimuthal angle ψ , while the polar angle is kept fixed at $\theta = 0$. Results of the scalar (left column, SD) and vector (right column, VD) descriptions of the incident Gaussian beam are compared for two vacuum wavelengths $\lambda_0 = 1064$ nm (solid curve) and $\lambda_0 = 700$ nm (dashed curve) corresponding to the NR alignment parallel (\parallel) and perpendicular (\perp) to the beam polarization (along x -axis), respectively. The stiffnesses are normalized to the unit incident power and calculated for Au NR ($l_L = 40$ nm, $l_S = 10$ nm) placed on the optical axis at its original stable longitudinal position z_0 (if no deflection is considered). The angular aperture is set to $\Theta = 50^\circ$.

stiffness, K_z changes sign for small NR deflections from the stable perpendicular orientation (\perp), and consequently the NR is repelled from z_0 longitudinally.

5. HEATING OF THE NANOROD

Since the absorption of the incident light causes heating of the NR that could destroy the NR or cause boiling of the liquid environment, we focus here on the temperature increase of the optically trapped NR. Seol *et al.* [48] assumed the following radial dependence for the temperature decrease outside the nanosphere (of radius R):

$$T(r) = T_0 + \Delta T \frac{R}{r}, \quad (55)$$

where r is the radial distance from the nanoparticle center, and ΔT is the temperature difference between the nanoparticle and the initial temperature T_0 . The light power absorbed by the object is equal to $P_{\text{abs}} = I(r_0)\sigma_{\text{abs}}$, where $I(r_0) = 1/2\epsilon_0 c n_m |\mathbf{E}(r_0)|^2$ is the irradiance of the object at the object position r_0 and $\sigma_{\text{abs}} = 3Vk\alpha_1''$ corresponds to the Rayleigh absorption cross-section of the object with volume V and polarizability α_1 (the index₁ signifies here only the dimensionless part of the polarizability; see below). In the steady state, the light power P_{abs} absorbed by the object is equal to the heat flow throughout the surface S of the object into the surrounding medium with thermal conductivity κ and refractive index n_m . Then the temperature rise of the NR can be expressed as [49]

$$\Delta T = \frac{I(r_0)\sigma_{\text{abs}}}{4\pi R\beta\kappa}, \quad (56)$$

where R corresponds to the radius of equivalent sphere having the same volume as the NR. Assuming an ellipsoidal NR with axes l_L, l_S, l_S , the following relation is valid: $(2R)^3 = l_L l_S^2$. The factor β strongly depends on the aspect ratio l_L/l_S , but it is very close to 1 for NRs with aspect ratios from 1 to 5. For a nanosphere, the dimensionless polarizability is expressed as

$$\alpha_1 = \frac{m^2 - 1}{m^2 + 2}, \quad (57)$$

while for an NR, we use the following expression:

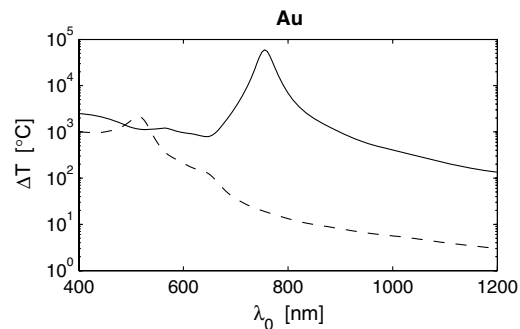
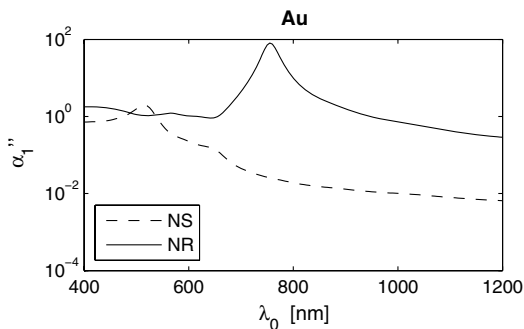


Fig. 10. Left: spectral dependence of the imaginary part of the polarizability α_1 for a gold nanosphere [$R = 16$ nm, dashed curve, Eq. (57)] and a gold ellipsoidal nanorod [$l_L = 40$ nm, $l_S = 10$ nm, solid curve, Eq. (58)] of the same volumes. Right: spectral dependence of the temperature increase for the same objects as in the left figure. The nanoparticles are immersed in water, and the electric field intensity at the beam focus is $E_0 = 19$ MV/m.

$$\alpha_1 = \frac{m^2 - 1}{3L(m^2 - 1) + 3}, \quad (58)$$

where L is done by Eq. (18) along one of the NR axes.

For the sake of consistency, we consider here the same intensity of the electric field at the beam focus $E_0 = 19$ MV/m as in the previous sections dealing with the optical trapping. This value is on average 1 order of magnitude higher compared to those used in the experimental optical manipulation with gold NRs [22,23]. Since optical force and also heating are linearly scalable with the incident power, the presented results can be easily rescaled to desired incident laser power. The effects of NR heating due to the absorption of the incident light are summarized in Fig. 10. The right part of Fig. 10 shows the temperature increase ΔT of a gold nanosphere and an NR of the same volume is placed at the beam focus. In reality, the nano-object is confined in an optical trap that is longitudinally displaced from the beam waist. At the trap location, the corresponding optical intensity is lower; however, the order of ΔT is not changed. Comparison of the spectral profile of NR heating with the spectral dependence of the imaginary part of the polarizability α_1 (Fig. 10, left) clearly shows the correlation of the two quantities. Figure 10 also confirms that the NR temperature increase is an order of magnitude higher compared to the nanosphere of the same volume. This is caused by a stronger polarizability α_1'' of the NR (see the left part of Fig. 10).

Based on the analytical expression (56), the temperature increase of the gold NR is enormous and water should boil there; however, it is not reported experimentally. Utilization of the finite element method gives the same results for the same NR. Recent theoretical results [50,51] based on the molecular dynamics provide an explanation based on the assumption that around a metallic nanoparticle there exists a thin fluid layer of high pressure and very low molecular density that could ensure nanoparticle melting without boiling of the surrounding liquid.

If the NR orientation θ is changed with respect to the polarization of the incident beam, the NR temperature decreases by several orders of magnitude (see Fig. 11). However, the NR is not optically confined in these orientations.

6. DISCUSSION

Even though we use the simplest theoretical description of the optical forces and torques acting upon metal NR, we find new

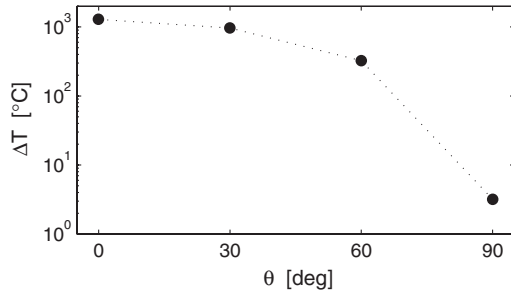


Fig. 11. Temperature increase of Au NR ($l_L = 40$ nm, $l_S = 10$ nm) illuminated at the wavelength $\lambda_0 = 850$ nm under different angles θ . The NR is immersed in water; the electric field at the beam focus is $E_0 = 19$ MV/m. These results were obtained by finite elements methods using Comsol Multiphysics software.

and interesting conclusions that are coherent with experimentally observed NR behavior.

Pelton *et al.* [22] reported stable trapping of a single gold NR ($l_L = 40$ nm, $l_S = 10$ nm) immersed in water. They used trapping wavelength 850 nm and objective lens with angular aperture 60 deg. Our results show that using the classical scalar description of the incident Gaussian beam one would not

be able to trap such NR. However, utilization of the more appropriate and precise vector description of the incident Gaussian beam predicts a potential well deep enough to provide stable confinement of the NR under the reported experimental conditions.

C. Selhuber-Unkel *et al.* measured lateral and longitudinal trap stiffnesses for an ensemble of gold NRs trapped on the optical axis [23]. Since the NR equilibrium position is independent of the incident trapping power and the trap stiffness is linearly proportional to the incident trapping power, they presented the trap stiffnesses normalized to the incident trapping power equal to 1 W. Taking their values and the NR parameters from Table 1 in [23], we calculated theoretically the normalized optical trap stiffnesses K_x , K_y , and K_z using the vector description of the incident Gaussian beam. The comparison between the experimental measurements [23] and our theoretical results is presented in Fig. 12. The theoretical results corresponding to the mean experimental values of the NR sizes (red \diamond) predict in general higher lateral stiffnesses; some results fit within the experimental error, but other results differ by an order of magnitude. In contrast to the lateral stiffness, the measured longitudinal trap stiffness K_z is

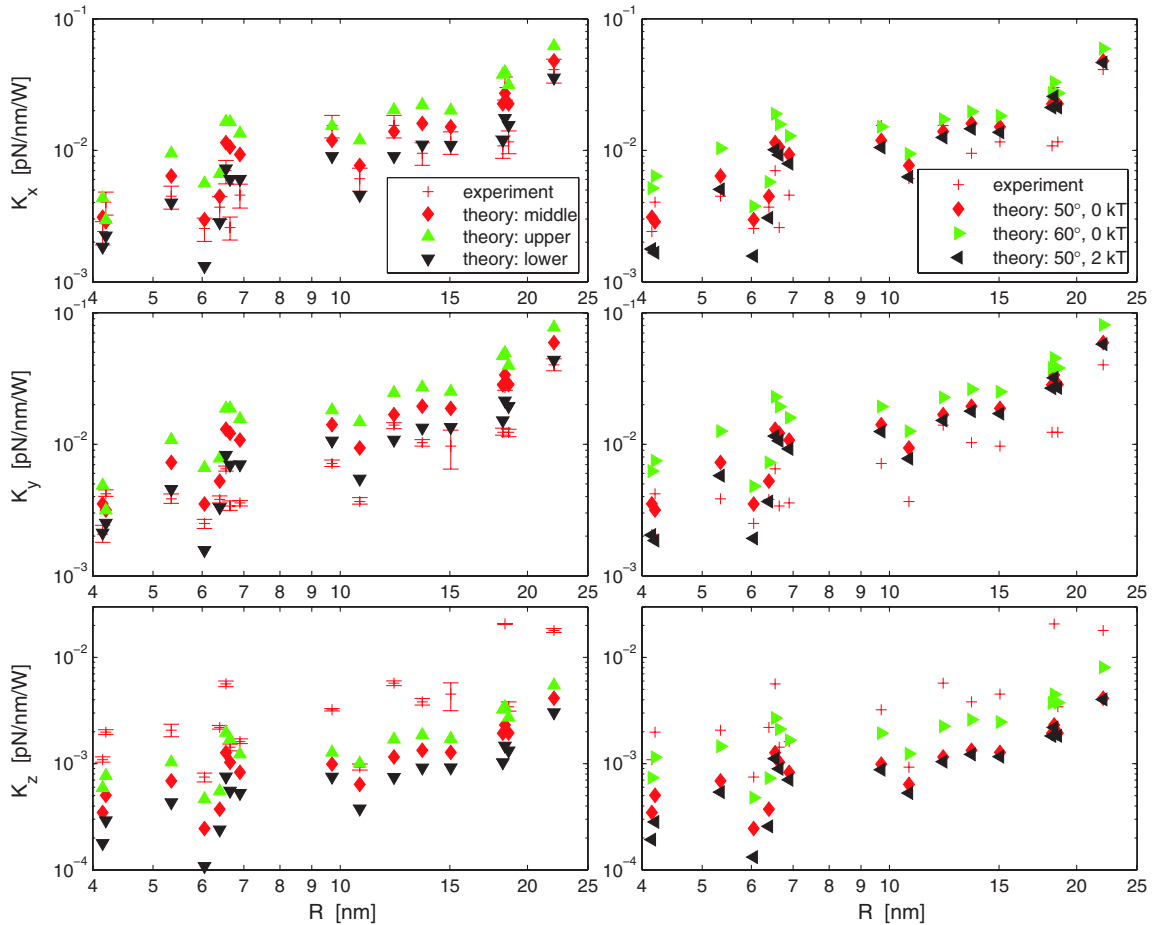


Fig. 12. (Color online) Comparison between the experimental trap stiffness measurements [23] and the theoretical predictions based on the vector description of the incident beam if the NRs are trapped on the optical axis at z_0 . The horizontal axis gives the mean value of the NRs radii $R = l_S/2$; both l_S and l_L of compared NRs are taken from Table 1 in [23]. The left column demonstrates the influence of the NR size on the stiffnesses. Here, \diamond denotes the theoretical results corresponding to the average measured values of the NR size and $\Theta = 50^\circ$; ∇ and Δ correspond to the smallest and biggest NRs within the experimental error reported in [23], respectively. The right column shows the dependence of the stiffness on the angular aperture Θ (\diamond versus \triangleright) and deflection of the NR from its equilibrium orientation corresponding to the reorientation work $U_R = 2kT$ (\diamond versus \triangleleft).

usually higher than the corresponding theoretical predictions. The above summary indicates that in this case, the expected vector description of the beam is not perfectly suitable for the experimental configuration. The reason for the discrepancy could stem from the fact that the authors used a special immersion oil with a carefully selected refractive index to suppress the spherical aberrations at the trapping plane placed $5\ \mu\text{m}$ above the lower cell surface and thus to maximize the longitudinal trap stiffness [23,52]. Such a procedure could lead to a field distribution with optimized and steeper intensity gradients in longitudinal direction but shallower gradients in the lateral direction, which corresponds to the results presented in Fig. 12. Obviously, to get a better coincidence with the theory, we would need to use a lower angular aperture Θ for the lateral stiffnesses and a higher aperture for the longitudinal stiffness, as the right column of the figure illustrates. The right column also shows that the deflection of the NR from its equilibrium orientation (corresponding to the work $U_R = 2k_B T$) does not influence the stiffnesses significantly. As illustrated in the left column, a stronger influence comes from the error in the experimental determination of the NR sizes. Here we plot the stiffness for the mean nanorod size and also for the smallest and biggest estimated nanorod sizes reported in Table 1 in [23]. It can be seen that the spread of the obtained stiffnesses is larger than the standard deviation of the mean of the experimental data.

Since the Rayleigh approximation is valid only for very small particles, its utilization for larger particles overestimates the optical forces [53]. Furthermore, we have not reduced the effective NR volumes due to the skin effect [4], which also results in overestimation of the optical forces. However, these trends are not clearly visible in Fig. 12.

The differences between the scalar and vector descriptions of the incident beam presented in the previous sections illustrated how strongly the spatial distribution of the field at the beam focus influences the stable NR confinement even if only one parameter Θ is used to characterize the beam. In this study, we have ignored all optical aberrations, even though they are likely to be responsible for the discrepancies between the measurement and simulation results presented in Fig. 12. The reason is that there is no exact procedure for how to obtain experimentally the spatial distribution of the electric field components at the beam focus to justify the proper theoretical description.

7. CONCLUSIONS

Within the Rayleigh approximation, we have presented a theoretical description of optical forces and torques acting upon a metal nanorod. To this end, we have adopted the scalar and vector descriptions of the focused Gaussian beam illuminating the NR and studied the behavior of metal NRs in respective fields. The analysis of the results has revealed that an NR can be aligned with its long axis parallel or perpendicular to the beam polarization, depending on the real parts of the NR polarizabilities along its long and short axis. We have demonstrated that a gold NR tends to orient its long axis parallel (perpendicular) to the beam polarization for laser wavelengths longer (shorter) than the longitudinal plasmon resonance wavelength. In the case of silver NRs, the behavior is more complex and the NR reorients at another two shorter

wavelengths close to the transversal plasmon resonant wavelength.

In addition, conditions for longitudinal and lateral optical trapping of a gold NR have been investigated. Vector description of the incident Gaussian beam predicts stable NR trapping even at low angular apertures and also at broader range of wavelengths. Only the vector description confirms stable optical trapping under the conditions observed experimentally [22]. Both models predict that it is not possible to trap gold NRs at wavelengths slightly longer than the plasmon resonant wavelength. Both models also predict a larger optical torque if the gold NR is illuminated by a wavelength slightly shorter than the plasmon resonant wavelength, even though the optical confinement is weaker here. The vector model also predicts unstable on-axial optical trapping of gold NRs at low angular apertures and wavelengths close to the plasmon resonance. Agreement in the order of magnitude has been reached with the experimental measurements of the NRs' lateral stiffnesses [23]. Even though the theoretical results differ from the experimental ones, they follow correctly the observed trend for NRs of different sizes, and the presented method enables rough and fast prediction of the NR behavior. The observed discrepancy is mainly caused by the lack of knowledge about the exact spatial distribution of the trapping electric field near the beam focus. A more versatile vector theoretical model would be more appropriate to simulate a tightly focused beam in real experiments [54].

ACKNOWLEDGMENTS

The authors acknowledge valuable comments of Dr. A. Jonáš and support from the Czech Scientific Foundation (202/09/0348), the Ministry of Education, Youth and Sports of the Czech Republic, and the European Commission (ALISI No. CZ.1.05/2.1.00/01.0017).

REFERENCES

1. K. C. Neuman and S. M. Block, "Optical trapping," *Rev. Sci. Instrum.* **75**, 2787–2809 (2004).
2. A. Jonáš and P. Zemánek, "Light at work: the use of optical forces for particle manipulation, sorting, and analysis," *Electrophoresis* **29**, 4813–4851 (2008).
3. J. R. Moffitt, Y. R. Chemla, S. B. Smith, and C. Bustamante, "Recent advances in optical tweezers," *Annu. Rev. Biochem.* **77**, 205–228 (2008).
4. K. Svoboda and S. M. Block, "Optical trapping of metallic Rayleigh particles," *Opt. Lett.* **19**, 930–932 (1994).
5. M. Dienerowitz, M. Mazilu, and K. Dholakia, "Optical manipulation of nanoparticles: a review," *J. Nanophoton.* **2**, 021875 (2008).
6. J. R. Arias-González and M. Nieto-Vesperinas, "Optical forces on small particles: attractive and repulsive nature and plasmon-resonance conditions," *J. Opt. Soc. Am. A* **20**, 1201–1209 (2003).
7. J. Pérez-Juste, I. Pastoriza-Santos, L. Liz-Marzán, and P. Mulvaney, "Gold nanorods: synthesis, characterization and applications," *Coord. Chem. Rev.* **249**, 1870–1901 (2005).
8. L. Tong, V. Miljković, and M. Käll, "Alignment, rotation, and spinning of single plasmonic nanoparticles and nanowires using polarization dependent optical forces," *Nano Lett.* **10**, 268–273 (2010).
9. P. H. Jones, F. Palmisano, F. Bonaccorso, P. G. Gucciardi, G. Calogero, A. C. Ferrari, and O. M. Maragò, "Rotation detection in light-driven nanorotors," *ACS Nano* **3**, 3077–3084 (2009).
10. W. Shelton, K. Bonin, and T. Walker, "Nonlinear motion of optically torqued nanorods," *Phys. Rev. E* **71**, 036204 (2005).
11. C. Sönnichsen and A. Alivisatos, "Gold nanorods as novel non-bleaching plasmon-based orientation sensors for polarized single-particle microscopy," *Nano Lett.* **5**, 301–304 (2005).

12. D. Higgins and B. Luther, "Watching molecules reorient in liquid crystal droplets with multiphoton-excited fluorescence microscopy," *J. Chem. Phys.* **119**, 3935–3942 (2003).
13. R. Yasuda, H. Noji, M. Yoshida, K. Kinoshita, and H. Itoh, "Resolution of distinct rotational substeps by submillisecond kinetic analysis of F-1-ATPase," *Nature* **410**, 898–904 (2001).
14. Z. Bryant, M. Stone, J. Gore, S. Smith, N. Cozzarelli, and C. Bustamante, "Structural transitions and elasticity from torque measurements on DNA," *Nature* **424**, 338–341 (2003).
15. B. Chithrani, A. Ghazani, and W. Chan, "Determining the size and shape dependence of gold nanoparticle uptake into mammalian cells," *Nano Lett.* **6**, 662–668 (2006).
16. R. Fan, R. Karnik, M. Yue, D. Li, A. Majumdar, and P. Yang, "DNA translocation in inorganic nanotubes," *Nano Lett.* **5**, 1633–1637 (2005).
17. J. Plewa, E. Tanner, D. Mueth, and D. Grier, "Processing carbon nanotubes with holographic optical tweezers," *Opt. Express* **12**, 1978–1981 (2004).
18. K. Bonin, B. Kourmanov, and T. Walker, "Light torque nanoscale control, nanomotors and nanorockers," *Opt. Express* **10**, 984–989 (2002).
19. L. Oroszi, P. Galajda, H. Kirei, S. Bottka, and P. Ormos, "Direct measurement of torque in an optical trap and its application to double-strand DNA," *Phys. Rev. Lett.* **97**, 058301 (2006).
20. F. C. Cheong and D. G. Grier, "Rotational and translational diffusion of copper oxide nanorods measured with holographic video microscopy," *Opt. Express* **18**, 6555–6562 (2010).
21. P. V. Ruijgrok, N. R. Verhart, P. Zijlstra, A. L. Tchebotareva, and M. Orrit, "Brownian fluctuations and heating of an optically aligned gold nanorod," *Phys. Rev. Lett.* **107**, 037401 (2011).
22. M. Pelton, M. Liu, H. Kim, G. Smith, P. Guyot-Sionnest, and N. Scherer, "Optical trapping and alignment of single gold nanorods by using plasmon resonances," *Opt. Lett.* **31**, 2075–2077 (2006).
23. C. Selhuber-Unkel, I. Zins, O. Schubert, C. Sönnichsen, and L. B. Oddershede, "Quantitative optical trapping of single gold nanorods," *Nano Lett.* **8**, 2998–3003 (2008).
24. E. Wolf, "Electromagnetic diffraction in optical systems. 1. An integral representation of the image field," *Proc. R. Soc. A* **253**, 349–357 (1959).
25. B. Richards and E. Wolf, "Electromagnetic diffraction in optical systems. 2. Structure of the image field in an aplanatic system," *Proc. R. Soc. A* **253**, 358–379 (1959).
26. J. J. Stamnes, *Waves in Focal regions* (IOP Publishing, 1986).
27. J. P. Barton and D. R. Alexander, "Fifth-order corrected electromagnetic field components for a fundamental Gaussian beam," *J. Appl. Phys.* **66**, 2800–2802 (1989).
28. P. Török, P. Varga, Z. Laczik, and G. R. Booker, "Electromagnetic diffraction of light focused through a planar interface between materials of mismatched refractive indices: An integral representation," *J. Opt. Soc. Am. A* **12**, 325–332 (1995).
29. A. E. Siegman, *Lasers* (University Science Books, 1986).
30. J. P. Barton, D. R. Alexander, and S. A. Schaub, "Theoretical determination of net radiation force and torque for a spherical particle illuminated by a focused laser beam," *J. Appl. Phys.* **66**, 4594–4602 (1989).
31. T. Nieminen, H. Rubinsztein-Dunlop, N. Heckenberg, and A. Bishop, "Numerical modelling of optical trapping," *Comput. Phys. Commun.* **142**, 468–471 (2001).
32. F. Borghese, P. Denti, R. Saija, and M. A. Iatì, "Optical trapping of nonspherical particles in the T-matrix formalism," *Opt. Express* **15**, 11984–11998 (2007).
33. A. A. R. Neves, A. Camoseo, S. Pagliara, R. Saija, F. Borghese, P. Denti, M. A. Iatì, R. Cingolani, O. M. Maragò, and D. Pisignano, "Rotational dynamics of optically trapped nanofibers," *Opt. Express* **18**, 822–830 (2010).
34. S. H. Simpson, D. C. Benito, and S. Hanna, "Polarization-induced torque in optical traps," *Phys. Rev. A* **76**, 043408 (2007).
35. F. Borghese, P. Denti, R. Saija, M. A. Iatì, and O. M. Maragò, "Radiation torque and force on optically trapped linear nanostructures," *Phys. Rev. Lett.* **100**, 163903 (2008).
36. P. C. Chaumet and C. Billaudeau, "Coupled dipole method to compute optical torque: application to a micropropeller," *J. Appl. Phys.* **101**, 023106 (2007).
37. C. Rockstuhl and H. Herzig, "Rigorous diffraction theory applied to the analysis of the optical force on elliptical nano- and microcylinders," *J. Opt. A* **6**, 921–931 (2004).
38. C. Rockstuhl and H. Herzig, "Calculation of the torque on dielectric elliptical cylinders," *J. Opt. Soc. Am. A* **22**, 109–116 (2005).
39. P. Chaumet and M. Nieto-Vesperinas, "Time-averaged total force on a dipolar sphere in an electromagnetic field," *Opt. Lett.* **25**, 1065–1067 (2000).
40. L. Novotny and B. Hecht, *Principles of Nano-Optics* (Cambridge University, 2006).
41. H. C. van de Hulst, *Light Scattering by Small Particles* (Dover, 1981).
42. D. Wang, S. Guo, H. Ren, and S. Yin, "Optical characteristics of silver-doped polarizing glass," *Opt. Lett.* **27**, 992–994 (2002).
43. F. Xu, J. A. Lock, G. Gouesbet, and C. Tropea, "Radiation torque exerted on a spheroid: analytical solution," *Phys. Rev. A* **78**, 013843 (2008).
44. E. Palik and G. Ghosh, *Handbook of Optical Constants of Solids*, Vol. 3, in *Handbook of Optical Constants of Solids* (Academic Press, 1998).
45. C. W. Gardiner, *Handbook of Stochastic Methods* (Springer-Verlag, 2004).
46. H. A. Kramers, "Brownian motion in the field of force and the diffusion model of chemical reactions," *Physica (Amsterdam)* **7**, 284–304 (1940).
47. S. H. Simpson and S. Hanna, "First-order nonconservative motion of optically trapped nonspherical particles," *Phys. Rev. E* **82**, 031141 (2010).
48. Y. Seol, A. E. Carpenter, and T. T. Perkins, "Gold nanoparticles: enhanced optical trapping and sensitivity coupled with significant heating," *Opt. Lett.* **31**, 2429–2431 (2006).
49. G. Baffou, R. Quidant, and F. J. García de Abajo, "Nanoscale control of optical heating in complex plasmonic systems," *ACS Nano* **4**, 709–716 (2010).
50. S. Merabia, P. Keblinski, L. Joly, L. J. Lewis, and J.-L. Barrat, "Critical heat flux around strongly heated nanoparticles," *Phys. Rev. E* **79**, 021404 (2009).
51. O. Ekcici, R. K. Harrison, N. J. Durr, D. S. Eversole, M. Lee, and A. Ben-Yakar, "Thermal analysis of gold nanorods heated with femtosecond laser pulses," *J. Phys. D* **41**, 185501 (2008).
52. S. N. S. Reihani and L. B. Oddershede, "Optimizing immersion media refractive index improves optical trapping by compensating spherical aberrations," *Opt. Lett.* **32**, 1998–2000 (2007).
53. Y. Harada and T. Asakura, "Radiation forces on a dielectric sphere in the Rayleigh scattering regime," *Opt. Commun.* **124**, 529–541 (1996).
54. M. J. Nasse and J. Woehl, "Realistic modeling of the illumination point spread function in confocal scanning optical microscopy," *J. Opt. Soc. Am. A* **27**, 295–302 (2010).